

# Tracing the Nature of Dark Energy with Galaxy Distribution

P. Solevi<sup>1,2</sup> <sup>\*</sup>, R. Mainini<sup>1,2</sup>, S.A. Bonometto<sup>1,2</sup>, A.V. Macciò<sup>3</sup>, A. Klypin<sup>4</sup> & S. Gottlöber<sup>5</sup>

<sup>1</sup> *Physics Department G. Occhialini, Università degli Studi di Milano–Bicocca, Piazza della Scienza 3, I20126 Milano (Italy)*

<sup>2</sup> *I.N.F.N., Sezione di Milano (Italy)*

<sup>3</sup> *Institute for Theoretical Physics, University of Zürich, Winterthurerstrasse 190, CH–8057 Zürich (Switzerland)*

<sup>4</sup> *Astronomy Department, New Mexico State University, Box 30001, Department 4500, Las Cruces, NM 88003-0001*

<sup>5</sup> *Astrophysikalisches Institut Potsdam, An der Sternwarte 16,14482 Potsdam (Germany)*

29 November 2018

## ABSTRACT

Dynamical Dark Energy (DE) is a viable alternative to the cosmological constant. Yet, constructing tests to discriminate between  $\Lambda$  and dynamical DE models is difficult because the differences are not large. In this paper we explore tests based on the galaxy mass function, the void probability function (VPF), and the number of galaxy clusters. At high  $z$  the number density of clusters shows large differences between DE models, but geometrical factors reduce the differences substantially. We find that detecting a model dependence in the cluster redshift distribution is a hard challenge. We show that the galaxy redshift distribution is potentially a more sensitive characteristics. We do so by populating dark matter halos in  $N$ -body simulations with *galaxies* using well-tested Halo Occupation Distribution (HOD). We also estimate the Void Probability Function and find that, in samples with the same angular surface density of galaxies in different models, the VPF is almost model independent and cannot be used as a test for DE. Once again, geometry and cosmic evolution compensate each other. By comparing VPF's for samples with fixed galaxy mass limits, we find measurable differences.

**Key words:** methods: analytical, numerical – galaxies: clusters – cosmology: theory – dark energy

## 1 INTRODUCTION

High redshift supernovae, anisotropies of the cosmic microwave background (CMB), as well as data on the large-scale galactic distribution (Riess et al. 1988, Perlmutter et al 1988, Tegmark et al. 2001, De Bernardis et al 2000, Hanany et al 2000, Halverson et al 2001, Spergel et al 2003, Percival et al. 2002, Efstathiou et al 2002) indicate that  $\sim 70\%$  of the world contents are due to a smooth component with largely negative pressure. This component is dubbed dark energy (DE). Recently Macciò, Governato & Horellou (2005) presented further arguments in favor of DE based on the local ( $\sim 5$ Mpc) Hubble flow of galaxies. The nature of DE is still open for debate. Candidates range from a positive cosmological constant  $\Lambda$  – yielding a  $\Lambda$ CDM cosmology – to models with a slowly evolving self-interacting scalar field  $\phi$  (dynamical DE; Ratra & Peebles 1988; Wetterich 1988) to

even more exotic physics of extra dimensions (e.g., Dvali & Turner 2003).

$\Lambda$ CDM cosmologies are easy to study and fit most data. Unfortunately, to give a physical motivation to the value of  $\Lambda$ , we need a *fine-tuning* of vacuum energy at the end of the last phase transition. To rival the success of  $\Lambda$ CDM other DE models ought to predict observables hardly distinguishable from it, so that discriminatory tests on DE nature are not easy to devise.

Up to now, most tests based on large scale structure dealt with the evolution of the cluster distribution. Using the Press-Schechter-type approximations (Press & Schechter 1974, PS hereafter; Sheth & Tormen, 1999, 2002 ST; Jenkins 2001) the expected dependence of the cluster mass function on DE nature was extensively studied (see, e.g., Wang & Steinhardt 1998, Haiman et al 2001, Majumdar & Mohr 2003, Mainini, Macciò & Bonometto 2003). The results were used to predict the redshift dependence of various observables, such as temperatures ( $T$ ) or photon counts ( $N$ ). In Sec. 2, we compare the (virial) mass functions for different

\* E-mail: solevi@mib.infn.it

DE. An important – and often overlooked – factor is the dependence of halo concentration  $c$  on the DE equation of state. For given virial mass the concentration varies with DE nature up to 80 %, as shown by simulations (Klypin, Macciò, Mainini & Bonometto 2003; Linder & Jenkins 2003; Kuhlen et al. 2005). The model dependence of  $c$  is so strong that it can be used as a possible discriminatory test for strong lensing measurements (Dolag et al 2004, Macciò 2005).

In this paper we shall focus on galactic  $\sim 10^{12} h^{-1} M_{\odot}$  scales which are also interesting for testing models of DE. In order to make a prediction we first need to know how to generate a distribution of galaxies, not just dark matter halos. There are different ways for doing this. We decided to use recent results on the Halo Occupation Distribution (HOD): a probability to find  $N$  galaxies in a halo of mass  $M$ . The HOD properties have been studied in details (Seljak 2000; Benson 2001; Bullock, Wechsler & Somerville 2002; Zheng et al. 2002; Berlind & Weinberg 2002; Berlind et al. 2003; Magliocchetti & Porciani 2003, Yang, van den Bosch & Mo 2003; van den Bosch, Yang & Mo 2003). Numerical simulations including gas dynamics (White, Hernquist & Springel 2001; Yoshikawa et al., 2001; Pearce et al. 2001; Nagamine et al. 2001; Berlind et al. 2003, Yang et al. 2004) or semi-analytical models of galaxy formation (Kauffmann, Nusser & Steinmetz 1997; Governato et al. 1998; Kauffmann et al. 1999a,b; Benson et al. 2000a,b; Sheth & Diaferio 2001; Somerville et al. 2001; Wechsler et al. 2001; Benson et al. 2003a; Berlind et al. 2003) were used, to find a law telling us how halos split in sub-halos hosting individual galaxies.

In this way we formulate predictions on galaxy mass functions and their  $z$ -dependence. In order to compare predictions with data we then need to disentangle the evolution of the mass function from the evolution of the  $M/L$  ratio, because observations provide luminosities of galaxies and our estimates give us halo masses. In this respect, one of the aims of this work is to estimate how precisely the  $M/L$  evolution should be known, in order to use data on galactic scales to test DE nature. Potentially,  $M/L$  evolution can be predicted using galactic evolution models (see, e.g., Bressan, Chiosi & Fagotto 1994, Portinari, Sommer-Larsen & Tantalo 2004, and references therein). Such predictions can be compared with weak lensing results or satellite dynamics (Prada et al 2003). The latter methods will provide estimates of virial  $M/L$  for samples of galaxies at different  $z$ . This is exactly what we need in order to test different models for DE. Here we find that, for some statistics, the expected signal, *i.e.*, the differences between models are rather large. So, there is a hope to detect DE effects in spite of uncertainties in  $M/L$  ratios. Certainly, if galactic evolution predictions and high- $z$   $M/L$  estimates are compared, one can hardly prescind from taking into account accurately the impact of DE nature.

We run a series of  $N$ -body simulations with different equations of state. In these models the ratio  $w = p_{de}/\rho_{de}$  of the DE pressure to the energy density varies with  $z$  according to field dynamics. The models considered here are the Ratra-Peebles (RP, Ratra & Peebles 1988) and the models with the supergravity (SUGRA, Brax & Martin 1999, 2001; Brax, Martin & Riazuelo, 2000). Appendix A gives a short summary on these models. Each model is specified by an additional parameter – the energy scale  $\Lambda$  of the self-interacting potential of the scalar field. Here we take

$\Lambda = 10^3 \text{ GeV}$  for both models. In RP (SUGRA),  $w$  shows slow (fast) variations with  $z$ .

The void probability function is an obvious candidate for discriminating models. Fluctuations grow differently in the models. So, one may expect some differences in VPF. We use galaxy distributions to estimate the void probability function (VPF) at different redshifts. While measuring VPF in simulations is straightforward, mimicking observations is slightly more complicated because it requires corrections for geometrical effects and because the answer depends on a definition of galactic populations. At  $z = 0$  no model dependence of the VPF is expected or found. Predictions at higher  $z$  depend on how galaxy samples are defined. In particular, we show that, if equal angular density samples are considered, VPF results are independent of the DE nature. On the contrary, if we select samples above fixed galactic mass  $M$ , a significant signal is found, which can be useful for testing the DE nature.

The plan of the paper is as follows: In Sec. 2 we discuss how geometry and galactic evolution affect the redshift distributions of galaxies and clusters. In Sec. 3 and 4 we discuss the simulations and prescriptions of populating halos with galaxies. In Sec. 5 and 6 results on redshift distributions and the VPF are given. Sec. 7 is finally devoted to discussing our results and future perspectives.

## 2 GEOMETRICAL AND EVOLUTIONARY FACTORS

Let us consider a set of objects whose mass function is  $n(> M, z)$ . In a spatially flat geometry, their number between  $z$  and  $z + \Delta z$ , in a unit solid angle, is given by

$$N(> M, z, \Delta z) = \int_z^{z+\Delta z} dz' D(z') r^2(z') n(> M, z') \quad (1)$$

with  $D(z) = dr/dz$ . For flat models:

$$D(z) = \frac{c}{H_o} \sqrt{\frac{\Omega_m(z)}{\Omega_{mo}(1+z)^3}}, \quad r(z) = \int_0^z dz' D(z') \quad (2)$$

Here  $\Omega_m(z)$  is the matter density parameter at the redshift  $z$ . The Friedman equation can be written in the form

$$H^2(z) = \frac{8\pi}{3} G \frac{\rho_{mo}(1+z)^3}{\Omega_m(z)} = H_o^2 \frac{\Omega_{mo}(1+z)^3}{\Omega_m(z)}. \quad (3)$$

Along the past light cone,  $a dr = -c dt$ . So, by dividing the two sides by  $dz = -da/a^2$ , one finds that  $a dr/dz = a^2 c dt/da$ . Accordingly,  $D(z) = dr/dz = c/H(z)$  is derived from eq. (3).

When  $w$  is a constant, a useful expression

$$D^2(z) = (c/H_o)(1+z)^{-3} [\Omega_{mo} + (1 - \Omega_{mo})(1+z)^{3w}]^{-1} \quad (4)$$

can be obtained, which allows one to see that the geometrical factors increase both when  $w$  decreases and  $\Omega_{mo}$  decreases in models with  $w < 0$ .

An extension to dynamical DE can be performed either by using the interpolating expressions yielding  $\Omega_m(z)$ , for RP and SUGRA models, provided by Mainini et al (2003b) or, equivalently, through direct numerical integration. We obtain the geometrical factor  $r^2(z)D(z)$  shown in the upper panel of Fig. 1.

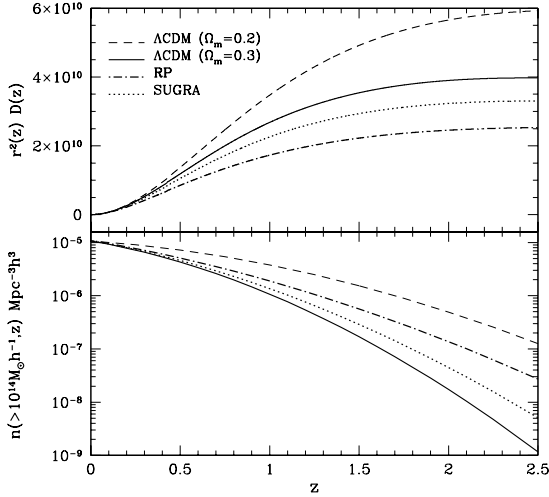


**Figure 1.** Geometrical and evolutionary terms on the cluster mass scale. In both panels  $\Lambda$ CDM with  $\Omega_{m0} = 0.2$  is above  $\Lambda$ CDM with  $\Omega_{m0} = 0.3$ . On the contrary, in the upper and lower panels RP and SUGRA lay on the opposite sides of  $\Lambda$ CDM. In the latter case, cancellation between geometrical and evolutionary effects is therefore expected.

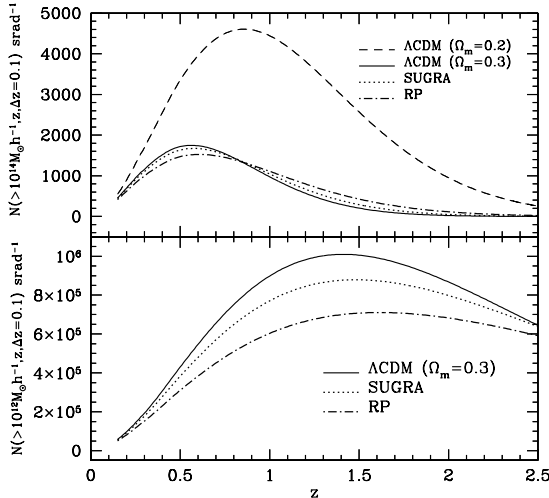


**Figure 2.** The upper panel shows how the redshift distribution on the cluster mass scale depends on the models. The cancellation expected from Fig. 1 has occurred and the models with  $\Omega_{m0} = 0.3$  are quite close, while  $\Lambda$ CDM grants large differences when varying  $\Omega_{m0}$ . In the lower panel, similar curves are shown for halos on galactic mass scales. In this case, evolution is almost model independent and the geometrical factor causes an appreciable difference. On these scales a lower  $\Omega_{m0}$  yields a different halo density, unless the spectrum is normalized to unphysical levels. Hence, only models with  $\Omega_{m0} = 0.3$  are shown.

Here  $\Omega_{m0} = 0.3$  or  $0.2$  for  $\Lambda$ CDM, while  $\Omega_{m0} = 0.3$  for SUGRA and RP models (for whom  $\Lambda = 10^3 \text{ GeV}$ ).  $H_0$  is  $70 \text{ km/s/Mpc}$  in all models ( $h = 0.7$ ). In the absence of number density evolution, the upper panel of Fig. 1 shows the dependence of the angular number density on  $z$ .

In the PS formulation, the expected differential cluster number density  $n(M)$ , at a given time, is then given by the expression

$$f(\nu)\nu d \log \nu = \frac{M}{\rho_m} n(M) M d \log M. \quad (5)$$

Here  $\rho_m$  is the matter density,  $\nu = \delta_c/\sigma_M$  is the *bias factor*,  $M$  is the mass scale considered.  $\sigma_M$  is the r.m.s. density fluctuation on the scale  $M$  and  $\delta_c$  is the amplitude that, in the linear theory, fluctuations have in order that, assuming spherical evolution, full recollapse is attained exactly at the time considered (in a standard CDM model this value is  $\sim 1.68$ ; the difference, in other model, ranges around a few percent). As usual, we took a Gaussian  $f(\nu)$  distribution.

Together with eq. (5), we must take into account the virialization condition, which yields significantly different density contrasts  $\Delta_v$  in different DE models. Further details can be found in Mainini et al (2003a).

In the lower panel of Fig. 1 we show the evolution of the number of halos of mass  $> 10^{14} h^{-1} M_\odot$ , in comoving volumes. All models are normalized to the same cluster number today and the redshift dependence of  $n(> M, z)$  is clearly understandable, on qualitative bases: When  $\Lambda$ CDM models are considered, the evolution is faster as we approach standard CDM. On the contrary, RP and SUGRA yield a slower evolution than  $\Lambda$ CDM.

The important issue is that, while both the geometrical factor and the evolutionary factor of  $\Lambda$ CDM (with  $\Omega_{m0} = 0.2$ ) lay above  $\Lambda$ CDM (with  $\Omega_{m0} = 0.3$ ), RP and SUGRA factors lay on the opposite sides of  $\Lambda$ CDM.

When the two factors are put together this causes the effect shown in the upper panel of Fig. 2, a strong signal on  $\Omega_{m0}$  and a widespread cancellation for DE models, compared to  $\Lambda$ CDM. Discriminating between different DE natures, from this starting point, is unavoidably a hard challenge.

Geometrical factors do not depend on the mass scale. Instead, evolutionary factors are known to have a stronger dependence on the model for larger masses. As cancellation is almost complete on cluster scales, it is to be expected that geometrical factors yield a significant signal on lower mass scales. This is shown on the lower panel of Fig. 2, where halos of  $10^{12} h^{-1} M_\odot$  are considered. A halos of this mass is expected to host a normal galaxy. More massive halos are expected to host many galaxies. Hence, this plot cannot be directly compared with observations. Its main significance is that such lower mass scales deserve to be inspected because DE signals are expected to be strong enough on these scales.

### 3 SIMULATIONS

The simulations run for this work are based on a  $\Lambda$ CDM model and two dynamical DE models, with the same matter density and Hubble parameters ( $\Omega_{m0} = 0.3$  and  $h = 0.7$ ). The simulations are run using the Adaptive Refinement Tree code (ART; Kravtsov, Klypin & Khokhlov 1997). The ART

code starts with a uniform grid, which covers the whole computational box. This grid defines the lowest (zereth) level of resolution of the simulation. The standard Particles-Mesh algorithms are used to compute density and gravitational potential on the zeroth-level mesh. The ART code reaches high force resolution by refining all high density regions using an automated refinement algorithm. The refinements are recursive: the refined regions can also be refined, each subsequent refinement having half of the previous level's cell size. This creates a hierarchy of refinement meshes of different resolution, size, and geometry covering regions of interest. Because each individual cubic cell can be refined, the shape of the refinement mesh can be arbitrary and match effectively the geometry of the region of interest.

The criterion for refinement is the local density of particles: if the number of particles in a mesh cell (as estimated by the Cloud-In-Cell method) exceeds the level  $n_{\text{thresh}}$ , the cell is split ("refined") into 8 cells of the next refinement level. The refinement threshold may depend on the refinement level. The code uses the expansion parameter  $a$  as the time variable. During the integration, spatial refinement is accompanied by temporal refinement. Namely, each level of refinement,  $l$ , is integrated with its own time step  $\Delta a_l = \Delta a_0 / 2^l$ , where  $\Delta a_0$  is the global time step of the zeroth refinement level. This variable time stepping is very important for accuracy of the results. As the force resolution increases, more steps are needed to integrate the trajectories accurately. Extensive tests of the code and comparisons with other numerical  $N$ -body codes can be found in Kravtsov (1999) and Knebe et al. (2000).

The code was modified to handle DE of different types, according to the prescription of Mainini et al. (2003b). Modifications include effects due to the change in the rate of the expansion of the Universe and on initial conditions, keeping into account also spatial fluctuations of the scalar field before they enter the horizon.

In this paper we use 4 new simulations. The models are normalized assuming  $\sigma_8 = 0.9$ . They are run in a box of  $100 h^{-1} \text{Mpc}$ . We use  $256^3$  particles with mass  $m_p = 4.971 \cdot 10^9 h^{-1} M_\odot$ . The nominal force resolution is  $3 h^{-1} \text{kpc}$ . All models are spatially flat, while  $\Omega_{m_0} = 0.3$  and  $h = 0.7$ . The two  $\Lambda\text{CDM}$  models start from different random numbers and are indicated as  $\Lambda\text{CDM1}$  and  $\Lambda\text{CDM2}$ . The two DE models, named RP3 and SUGRA3, are started from the same random numbers of  $\Lambda\text{CDM1}$ .

#### 4 GALAXIES IN HALOS

Halos made by more than 30 particles were found in simulations by the same spherical overdensity (SO) algorithm used in Klypin et al (2003). The algorithm locates all non-overlapping largest spheres where the density contrast attains a given value  $\Delta_v$ . Density contrasts are assigned the virialization values, which depend on the redshift  $z$  and on parameters of the DE. For instance, at  $z = 0$ ,  $\Delta_v = 101.0$  for  $\Lambda\text{CDM}$ , 119.4 for SUGRA3 and 140.1 for RP3;  $\Delta_v$  values for higher  $z$  can be found in Mainini, Macciò & Bonometto (2003; see also Mainini et al 2003b).

Figure 3 shows the halo mass function in the LCDM1, the SUGRA3, and the RP3 models at  $z = 0$ . Differences between the models are only due to different  $w(z)$ , while their

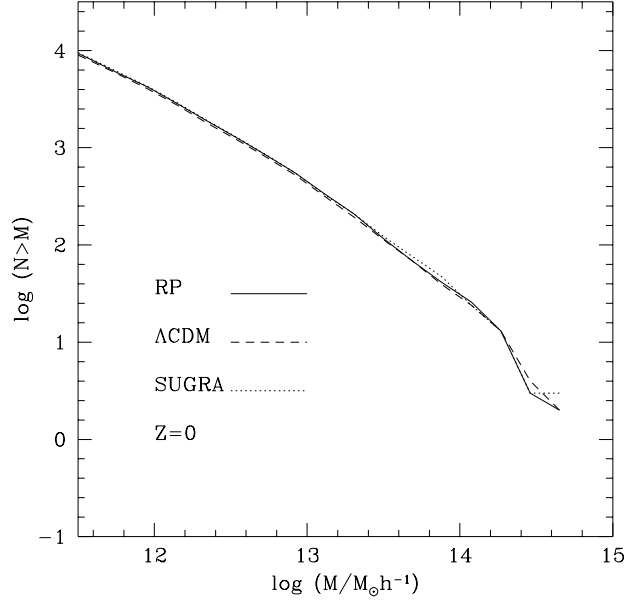


**Figure 3.** Halo mass function at  $z = 0$ . Results for  $\Lambda\text{CDM}$  (dashed line), RP (solid line), and SUGRA (dotted line) overlap.

$\sigma_8$  is identical. Accordingly, at  $z = 0$  their mass functions almost overlap and are well fitted by the Sheth-Tormen (ST, Sheth & Tormen, 1999) approximation.

However, when we consider galaxies, we need to use another approach because individual halos may host many galaxies of different mass and luminosity. In order to assign galaxies to halos we use a HOD. This is a relatively novel approach to locate galaxies in each halo. It can be used in different ways. Full-scale semi-analytical methods can predict such quantities as the luminosity, colors, star-formation rates. Unfortunately, many important mechanisms are still poorly understood making the results less reliable. It seems therefore advisable to minimize the physical input, keeping just to gravitational dynamics.

In this paper we use a prescription consistent with the results of Kravtsov et al (2004). We utilize an analytical expression recently proposed by Vale & Ostriker (2004), but parameters of the approximation are different from Vale & Ostriker (2004) and tuned to produce a good fit to results of Kravtsov et al (2004). The approximation is based on the assumption that the probability  $P_s(N_s|M)$  for a halo of mass  $M$  to host  $N_s$  subhalos is approximately universal. We take the Schechter approximation

$$N(m|M) dm = A \frac{dm}{\beta M} \left( \frac{m}{\beta M} \right)^{-\alpha} \exp\left(-\frac{m}{\beta M}\right) \quad (6)$$

for the number of subhaloes with masses in the range  $m$  to  $m + dm$ , for a parent halo of mass  $M$ .  $A$  must be such that the total mass in subhaloes,  $\int_0^\infty dm m N(m|M)$ , is a fraction  $\gamma M$  of the parent halo mass. Therefore  $A = \gamma / \beta \Gamma(2 - \alpha)$ , so that the number of sub-halos of mass  $m$  is

$$n_{sh}(m) = \int_0^\infty dM N(m|M) n_h(M), \quad (7)$$

( $n_h(M)$  is the halo mass function) independently from the

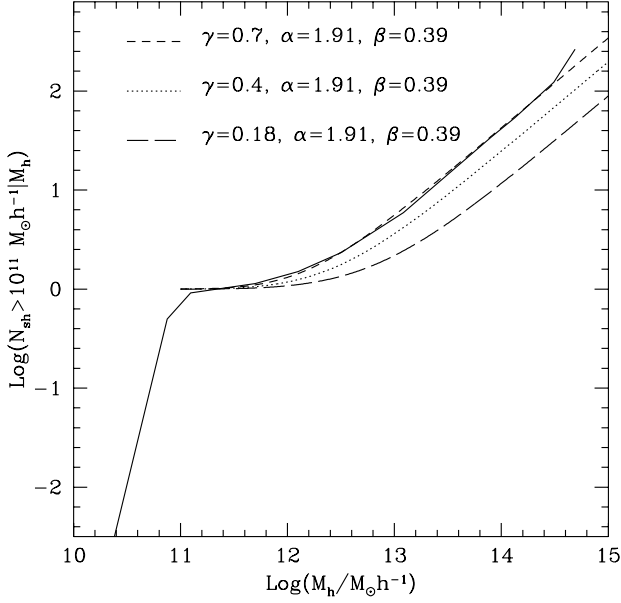


**Figure 4.** Comparison of different halo occupation distributions. The solid line is the HOD given by Kravtsov et al (2004). Other curves are obtained from eq.(8) for different parameters  $\gamma$  as indicated in the plot.

parent halo mass. The expression (6) yields the following number of subhaloes with mass  $> m$  in a halo of mass  $M$ :

$$N_{sh}(> m, M) = \frac{\gamma}{\beta\Gamma(2-\alpha)} \int_{m/\beta M}^{\infty} dx x^{-\alpha} \exp(-x). \quad (8)$$

Sub-haloes will be then identified with galaxies. Figure 4 shows that the expression approximates the results of Kravtsov et al (2004) once we fit parameters  $\alpha, \beta, \gamma$  and add to the expression (8) a unity, *i.e.* the halo as a sub-halo of itself. For large haloes, to be interpreted as galaxy clusters, this sub-halo could be the central cD; but adding an extra object, in such large galaxy sets, is just a marginal reset. For small haloes, instead, it is important not to forget that they represent a galaxy, as soon as they exceed the galaxy mass threshold.

In a different context, Vale & Ostriker (2004) use the value  $\gamma = 0.18, \beta = 0.39$ . Owing to the use we make of eq. (8),  $\gamma = 0.7$  appears more adequate.

If the (differential) halo mass function  $n_h(M)$  is known, the sub-halo mass function is

$$N_{sh}(> m) = \frac{\gamma}{\beta\Gamma(2-\alpha)} \times \int_{m/\gamma}^{\infty} dM n_h(M) \int_{m/\beta M}^{\infty} dx x^{-\alpha} \exp(-x). \quad (9)$$

If we perform nonlinear predictions,  $n_h(M)$  is obtained from the expression (5) or from the corresponding expressions in the ST case. When we deal with simulations, halo masses have discrete values  $m_\nu = \nu m_p$ , appearing  $n_h^{(\nu)}$  times, up to a top mass  $\nu_M m_p$ . Then

$$N_{sh}(> m) = \frac{\gamma}{\beta\Gamma(2-\alpha)} \times$$

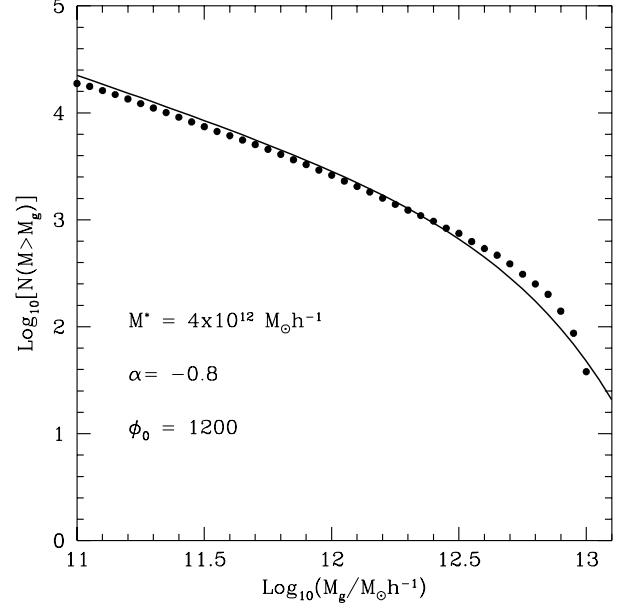


**Figure 5.** Galaxy (cumulative) mass function at  $z = 0$  from simulations (dots) *vs.* an integral Schechter function, with  $\Phi_0, \alpha$  and  $M_*$  shown in the frame.

$$\times \sum_{\nu=\frac{m}{\gamma m_p}}^{\nu_M} n_h^{(\nu)} \int_{\nu m/\beta M}^{\infty} dx x^{-\alpha} \exp(-x). \quad (10)$$

In Figure 5 we plot the galaxy mass function obtained with eq. (10), using the mass function of halos in the simulations, and identifying sub-haloes with galaxies. At  $z = 0$  model differences are unappreciable and the plotted function holds for all models. We also plot a Schechter function with the parameters shown in the frame, selected to minimize the ratios between differential values at all points. As expected, the two curves are close. In fact, there must be some relation between masses and luminosities, but the  $M_g/L_g$  ratio should not be a constant.

## 5 GALAXY ANGULAR DENSITY IN MODELS WITH DIFFERENT DE

Let us now consider the galaxy mass function at higher  $z$ , for the different models. According to eq. (1), the number of galaxies with mass  $> m$ , in a solid angle  $\Delta\theta^2$  ( $\Delta\theta \ll 1$ ), between redshifts  $z$  and  $z + \Delta z$ , is

$$\frac{N_g(> m, z; \Delta z, \Delta\theta)}{\Delta z \Delta\theta^2} \simeq c \frac{r^2(z)}{H(z)} n_g(> m, z), \quad (11)$$

if  $n_g(> m, z)$  is the comoving number density of galaxies with mass  $> m$  at a redshift  $z$ . The galaxy density can be obtained from the subhalo mass functions (9) and (10). Accordingly, the average angular distance  $\theta_{gg}$  is given by

$$\theta_{gg}(> m, z) \sqrt{\Delta z} \simeq \frac{1}{r(z)} \left[ \frac{H(z)}{n_g(> m, z)} \right]^{1/2}. \quad (12)$$

Thus, the l.h.s. expression is independent of the particular volume considered.

Such  $\theta_{gg}(> m, z)$  therefore depends on geometry, halo mass function and HOD. We however expect that the redshift dependence mostly arises from geometry, while evolution plays a significant role at higher  $z$ . In fact, the main difference between this and the cluster case is that evolution is mild and discrepancies between models, in comoving volumes, up to  $z \sim 2$ , are even weaker.

Let  $\theta_{\Lambda}(z)$ ,  $\theta_{SU}(z)$ ,  $\theta_{RP}(z)$  be the mean angular distances between galaxies at redshift  $z$  for the  $\Lambda$ CDM, SUGRA and RP models, respectively. Besides these functions, let us also consider the angular distance  $\theta_{geo}(z)$  obtained from eq. (12), keeping the value of  $n_g(> m, z=0)$  at any redshift and the  $\Lambda$ CDM geometry. Therefore,  $\theta_{geo}(z)$ , although the symbol has no reference to  $\Lambda$ CDM, describes the behavior of the angular separation *in a  $\Lambda$ CDM model*, in the limit of no halo evolution.

In Figure 6, we compare results obtained from simulations with the ST predictions in different models. Rather than presenting  $\theta_{mod}(z)$ , we plot the fractional difference  $(\theta_{mod} - \theta_{geo})/\theta_{geo}$ . In principle, error bars can be evaluated in two ways: (i) by comparing  $\Lambda$ CDM1 with  $\Lambda$ CDM2 (cosmic variance) and (ii) by comparing the differences between models. The latter can be done only at present because the models have the same power spectrum only at  $z=0$ . The differences between models exist because the fluctuations grow differently in the past. At larger  $z$ , this *evolutionary variance* should be smaller, but is not easy to evaluate. We use differences between models at  $z=0$  as a rough estimate of error bars at all redshifts. Judging by the differences between  $\Lambda$ CDM1 and  $\Lambda$ CDM2, the cosmic variance seems to be smaller by a factor of three than the evolutionary differences. We find similar behaviour for different galaxy masses. In all cases, differences between models can be clearly seen.

The largest differences between models are attained at  $z \sim 1$ . Let us remind that the plot shows the fractional differences between DE models and the  $z$ -dependence due to the mere  $\Lambda$ CDM geometry. At  $z \simeq 1$ , this difference is just  $\simeq 5\%$  for  $\Lambda$ CDM while, for SUGRA, it is  $\sim 20\%$ , because of the different geometry and a still slower cosmological evolution. Even larger is the difference with RP. This compares with an evolutionary variance hardly exceeding  $\sim 2\%$ , if the effective comoving volume inspected is  $\sim 10^6 h^{-3} \text{Mpc}^3$ . For  $\Delta z \sim 0.1$ , this corresponds to  $\delta\theta \sim 30\text{--}40^\circ$ .

The discriminating power of this theoretical prediction is to be still compared with two possible sources of error: (i) Peculiar velocities, setting individual galaxies into an apparent redshift band different from the one to which they belong. (ii) Luminosity evolution.

Overcoming the latter point is critical to the use of galaxies as indicators of DE nature and we shall devote the whole next section to the impact of luminosity evolution. The conclusion of this discussion is that galaxies are indeed a possible indicator of DE nature, but more work is needed before they can be efficiently used to this aim.

In this section we shall report the result of a test performed to evaluate the impact of redshift displacements due to peculiar velocities.

We divided the volume  $L^3$  of the box into cells of side  $10^{-1}L$ , with volume  $10^{-3}L^3$ . 50 such cells were selected at random at each redshift and replaced by the cells at the closest redshift considered with their galaxy contents. The redshift displacement between the original cell and its re-

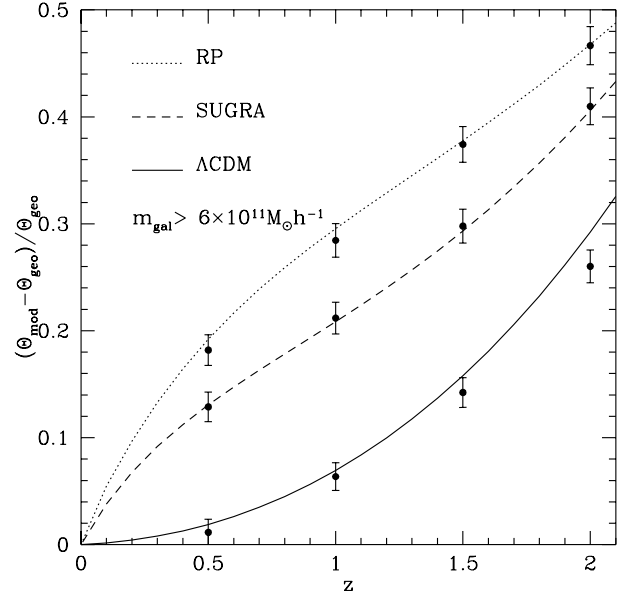


**Figure 6.** The redshift dependence of the mean fractional angular separation in different models. Points with error bars show results of simulations. Curves indicate ST predictions. The plot shows a strong dependence of the galaxy redshift distribution on the DE nature.

placements is  $\pm 0.5$ . For a change of 5% in galaxy contents the average shift of  $\theta_{gg}$  is  $\sim 1.2\%$ .

This shift lays well below the error bars shown in Figure 6. However, the average errors due to evolutionary and cosmic variance plus peculiar velocities are  $\sim 2.4\%$  and the whole error never exceeds 2.6–2.7%. We therefore argue that these sources of error do not affect the robustness of results.

## 6 DEPENDENCE ON MASS–LUMINOSITY RELATION

Let us now consider galaxy evolution, which is expected to cause  $z$ -dependence of the average  $M_g/L_g$  ratio, but can also yield a  $z$ -dependence of the  $M_g/L_g$  distribution about such average, in a way which may depend on the mass range considered. From an observational point of view, when we consider galaxies of various luminosities  $L_g$ , we must then take into account that their expected mass  $M_g$  could be distributed with different laws at different  $z$  and  $L_g$ .

Let us therefore consider the galaxy distribution on the  $M_g, L_g$  plane at a given  $z$ , yielding the galaxy number

$$dN = D(M_g, L_g, [z]) dM_g dL_g \quad (13)$$

in the infinitesimal area  $dM_g dL_g$  about the point  $M_g, L_g$ . We put  $z$  in brackets to outline that, in respect to it,  $D$  is not a *distribution* but a *function*. Obviously we expect a strong correlation between  $M_g$  and  $L_g$ , at any  $z$ , so that it makes sense to consider an average  $M_g/L_g$  ratio.

Once the distribution  $D$  is assigned, the distributions

on  $M_g$  (at fixed  $L_g$ ) and on  $L_g$  (at fixed  $M_g$ ) read

$$\phi(M_g, [z]) = \int dL_g D(M_g, L_g, [z]) ,$$

$$\psi(L_g, [z]) = \int dM_g D(M_g, L_g, [z]) .$$

The number  $dN$  is also the product of  $\phi(M_g, [z])$  times the distribution on luminosities at fixed mass  $M_g$ :

$$dN = \phi(M_g, [z]) Q(L_g; [M_g, z]) dM_g dL_g . \quad (14)$$

Equating the r.h.s.'s of eqs. (13) and (14) yields

$$Q(L_g; [M_g, z]) = \frac{D(M_g, L_g, [z])}{\int dl D(M_g, l, [z])} \quad (15)$$

and, similarly, the distribution on masses at given  $L_g$ , reads

$$P(M_g; [L_g, z]) = \frac{D(M_g, L_g, [z])}{\int dm D(m, L_g, [z])} . \quad (16)$$

We can now use  $P$  to work out the average  $M_g/L_g$  at fixed  $L_g$ , and the distribution on  $M_g/L_g$  about such average. Clearly

$$\begin{aligned} \left\langle \frac{M_g}{L_g} \right\rangle_{L_g, z} &= \frac{1}{L_g} \int dm m P(m; [L_g, z]) = \\ &= \frac{1}{L_g} \frac{\int dm m D(m, L_g, [z])}{\int dm D(m, L_g, [z])} , \end{aligned} \quad (17)$$

while the distribution

$$\mathcal{D}(M_g; [L_g, z]) = \frac{M_g}{L_g} \frac{D(M_g, L_g, [z])}{\int dm D(m, L_g, [z])} \quad (18)$$

tells us how  $M_g/L_g$  is distributed around  $\langle M_g/L_g \rangle_{L_g, z}$ .

The impact of the evolution of stellar populations (or other mechanisms) on the  $M_g/L_g$  ratio can be fully expressed through the distribution  $D(M_g, L_g; [z])$  in eq. (13). From it we can work out an average mass/luminosity ratio  $\langle M_g/L_g \rangle$  and the distribution on masses  $\mathcal{D}$ ; they both depend on  $L_g$  and  $z$ .

Let us now try to inspect how such variable  $\mathcal{D}$  distribution affects our results, taking into account that we mostly ignore how such variations occur. Accordingly, we shall proceed as follows: we define a “wild” distribution, that we expect to spread the  $M_g/L_g$  ratio, at fixed  $L_g$ , farther from average than any physical  $\mathcal{D}$ , at any  $z$ , will do. The effects caused by such wild distribution should then be an overestimate of the effects of the actual distributions. Should they cause just a minor perturbation in estimates, all we have to worry about is the redshift dependence of the average  $\langle M_g/L_g \rangle_{L_g}$ .

More in detail, we shall allow that a galaxy of given mass  $M_g$  has a luminosity in an interval  $L_1, L_2$  with  $L_2 \sim 20 L_1$ . We test this prescription without direct reference to luminosities: In the sample of galaxies obtained through the HOD, at each  $z$ , each galaxy mass ( $m$ ) is replaced by a mass  $m' = m + \Delta m R$ ,  $R$  being a random number with normal distribution and unit variance. We take  $\Delta m = 0.8 m$ , but replace all  $m' < 0.1 m$  with  $0.1 m$ , as well as all  $m' > 1.9 m$  with  $1.9 m$ . The shift is therefore symmetric on  $m$  (not on  $\log m$ ). The operation causes a slight increase of the mass function above  $\bar{M} \sim 2.8 \cdot 10^{11} h^{-1} M_\odot$  (by a few percents),

as there are however more lighter galaxies coming upwards than heavier galaxies going downwards (below  $\bar{M}$ , the low-mass cut-off of the mass function, set by the mass resolution of our simulations – see section 3 – begins to cause shortage of transfers upwards). The operation is then completed by reducing all masses by a (small) constant factor, so that, summing up all masses of objects with mass  $M_g > \bar{M}$ , we have the same total mass as before the operation. This lowers the limit below which the mass function preserves its initial shape, but we never use galaxy samples including masses below  $3 \cdot 10^{11} h^{-1} M_\odot$ .

We re-estimated  $\theta_{mod} \sqrt{\Delta z}$  using the new masses, for the same mass limits as before, and compare the changes obtained in this way with the Poisson uncertainty, due to the finite number of galaxies in each sample.

We find that the error obtained from the above procedure ranges between 20 and 40% of the Poisson error.

This output tells us that the evolution of the physical distribution can be expected to redistribute results well inside Poisson uncertainty. If we expect this redistribution to be random, the top value of the whole expected error is then 3%; if we attribute a systematic character to it and refrain from performing a quadratic sum with the other error sources considered, the overall possible error is still within 3.8%. It should be outlined that here we pushed all error sources to their maximum; thus, we believe that the above estimates are safely conservative.

Let us now discuss how the evolution of the average  $M_g/L_g$  ratio can affect the use of galaxies to detect DE nature. In principle, one could use the  $z$  dependence of  $D(M_g, L_g)$ , to obtain the  $z$ -dependence of the  $\langle M_g/L_g \rangle_{L_g}$  ratio. More realistically, suitable data sets can directly provide the  $z$ -dependence of  $\langle M_g/L_g \rangle_{L_g}$ , with some residual uncertainty. The basic issue is then: How well the  $z$  evolution of  $\langle M_g/L_g \rangle_{L_g}$  is to be known, in order that we can test DE nature?

Figure 6 is however devised so to provide a direct reply to this question: If we double the values of  $\delta\theta_{gg}/\theta_{gg}$  provided there, we have a fair estimate the difference between evolution rates of  $\mathcal{R} = \langle M_g/L_g \rangle_{L_g}(z)/\langle M_g/L_g \rangle_{L_g}(z=0)$  needed just to cover the differences between geometry and dynamics for the  $\Lambda$ CDM model or to compensate the differences between the  $\Lambda$ CDM geometry and whole evolution for dynamical DE models, (in the limit  $M_g \ll M_*$ , where  $M_*$  is the mass scale appearing in a Schechter-like expression). Figure 6 can just be interpreted in both senses, changing the name of the ordinate.

For instance, at  $z = 0.5$ , an uncertainty  $\sim 20\%$  (35%) on the evolution of  $M_g/L_g$  is needed to hide the difference between  $\Lambda$ CDM and SUGRA (RP).

Let us show this point. Owing to eq. (12),  $\theta_{gg} \propto n_g^{-1/2}$ , so that a shift  $\delta\theta_{gg}$  in the observed angular distance arises from a shift

$$\frac{\delta n_g}{n_g} \simeq 2 \frac{\delta\theta_{gg}}{\theta_{gg}} \quad (19)$$

in the galaxy number density

$$n_g(> M_g) = n_g \left( > L_g \frac{M_g}{L_g} \right) . \quad (20)$$

The latter shift, as shown in eq. (20), can arise from a shift on  $M_g/L_g$ , being

$$\delta n_g = n_g(M_g)L_g \delta \left( \frac{M_g}{L_g} \right); \quad (21)$$

here  $n_g(M_g)$  is the differential mass function, obtained by differentiating the integral mass function  $n_g(> M_g)$ . Therefore,

$$\frac{\delta n_g(> M_g)}{M_g n_g(M_g)} \simeq \frac{\delta(M_g/L_g)}{(M_g/L_g)} \quad (22)$$

and

$$\frac{\delta(M_g/L_g)}{(M_g/L_g)} \simeq \frac{\delta n_g(> M_g)}{n_g(> M_g)} \frac{n_g(> M_g)}{M_g n_g(M_g)}. \quad (23)$$

If we approximate the integral mass function by a Schechter expression, it is  $|m n(m)/n(> m)| = 1 + m/M_*$ , so that

$$\frac{\delta(M_g/L_g)}{(M_g/L_g)} \simeq \frac{\delta n_g(> M_g)}{n_g(> M_g)} \left( 1 + \frac{M_g}{M_*} \right)^{-1}. \quad (24)$$

Using this equation together with eqs. (19) and (23), we have the relation

$$\frac{\delta(M_g/L_g)}{(M_g/L_g)} \simeq 2 \left( 1 + \frac{M_g}{M_*} \right)^{-1} \frac{\delta \theta_{gg}}{\theta_{gg}} \quad (25)$$

telling us how to use Figure 6 to estimate the evolution of  $M_g/L_g$  needed to yield the same effects of a change in DE nature. This equation also tells us how to use Figure 6 for masses approaching  $M_*$ .

## 7 THE VOID PROBABILITY FUNCTION

Let us randomly throw spheres of radius  $R$ , in a space where objects of various masses  $M$  are set. The probability  $P_o(R)$  of finding no object with  $M > M_{tr}$  in them, if the VPF for objects of mass  $> M_{tr}$ .

We expect and find no model dependence in the *galaxy* VPF's at  $z = 0$ . At  $z > 0$ , a critical issue is how  $M_{tr}$  is set. One can simply plan to determine the galaxy masses  $M_g$  from data (e.g., from  $L_g$  values), so to select galaxies with  $M_g > M_{tr}$ . As widely outlined, this choice involves several complications. Another option is taking the most *luminous* galaxies up to an average angular distance  $\theta_{gg}$ .

Each threshold  $M_{tr}$ , for any  $z$  and  $\Delta z$ , yields a value of  $\theta_{gg}$ . Fig. 6 shows how  $\theta_{gg}$  depends on the model at fixed threshold. *Viceversa*, if we keep, for that  $z$  and  $\Delta z$ , a fixed  $\theta_{gg}$ , the relative  $M_{tr}$  varies with models. We can compare models either at fixed  $M_{tr}$  or at fixed  $\theta_{gg}$ . Dealing with observations, the latter option is easier, but mixes up the intrinsic VPF dependence on the model and other features, which also depend on the model.

Besides of threshold setting, another issue bears a great operational relevance. In principle, VPF's can be evaluated in the comoving volumes where galaxies are set and compared there with VPF's from data. This is however inadequate to evaluate how discriminatory is the VPF statistics. To do so, we rather follow the following steps:

- (i) From cartesian coordinates  $\bar{x}_i$  ( $i = 1, 2, 3$ ) in comoving volumes we work out the redshift and the celestial coordinates  $z, \theta, \phi$  that an observer, set at  $z = 0$ , would measure. This is done by using the geometry of the model.
- (ii) Data also give  $z, \theta, \phi$ , for each galaxy. But, to estimate the VPF, they must be translated into cartesian coordinates  $x_i$ . An observer can only perform such translation by using

the geometry of a *fiducial* model, e.g.,  $\Lambda$ CDM. The second step, to forge predictions, therefore amounts to re-transform  $z, \theta, \phi$  into cartesian coordinates  $x_i$ , but using now the *fiducial*  $\Lambda$ CDM geometry;  $x_i$ 's coincide with the  $\bar{x}_i$ 's only for a  $\Lambda$ CDM cosmology. Let us call *fiducial* space, the environment where galaxies are now set.

(iii) We then estimate the VPF's, for all models, in the fiducial space; these VPF's should be compared with observational data, but can also be compared one another to assess how discriminatory this statistics can be.

Although comparing predictions for VPF's in comoving volumes, therefore, bears little discriminatory meaning, our outputs are more easily explained if we start from comoving space VPF's. Let us recall that, on galaxy scales, evolutionary differences, up to  $z \sim 2$ , are modest. Accordingly, for an assigned  $M_{tr}$ , we find just marginal discrepancies, as is shown in Fig. 7 for  $M_{tr} = 6 \cdot 10^{11} M_\odot h^{-1}$ . Differences among VPF's arise, of course, if we do not fix  $M_{tr}$ , but  $\theta_{gg}$ , as a reflex of  $\theta_{gg}$  differences. These VPF's are shown in Fig. 8.

VPF's in respect of comoving coordinates bear a strict analogy with mass functions in comoving volumes. The fact that geometry erases almost any signal on the cluster mass function is analogous to what happens for the VPF, when we pass from the comoving to the fiducial space. This fact is far from trivial. Let us compare these VPF's with the VPF's in a Poisson sample with the same  $\theta_{gg}$  (Fig. 10) and remind that (White 1979)

$$P_o(R) = \exp \left[ -\bar{N}_R + \sum_{n=2}^{\infty} \frac{(-\bar{N}_R)^n}{n!} \xi^{(n)}(R) \right]. \quad (26)$$

Here  $\bar{N}_R$  is the average number of points in a sphere of radius  $R$ ;  $\xi^{(n)}(R)$  are the  $n$ -point functions averaged within the same sphere. For the Poisson sample  $P_o(R) = \exp(-\bar{N}_R)$ , as all  $\xi^{(n)}(R)$  vanish. The difference between Poisson VPF and model VPF is to be fully ascribed to  $\xi^{(n)}$ , as  $\bar{N}_R$  is set equal. This difference is huge, in respect to the differences between models, which should arise because of  $\xi^{(n)}$  shifts. Their paucity indicates that density renormalization almost erases the shifts in correlation functions of all orders.

The cancellation between geometrical and  $\theta_{gg}$  effects, shown in Fig. 9, indicates that the passage from comoving to fiducial coordinates bears a weight comparable with the differences shown in Fig. 8. It therefore comes as no surprise that VPF's, for fixed  $M_{tr}$ , almost absent in the comoving space, are significant in the fiducial space. They are shown in Fig. 11 and, as is expected, the curves of different models appear in the opposite order in respect to Fig. 8.

If the redshift dependence of the  $M_g/L_g$  ratio is under control, Fig. 11 shows a discriminatory prediction which can be compared with data. Once again, the problem concerns both the evolution of the mean  $M_g/L_g$  ratio and single galaxy deviations from average. Supposing that the average  $M_g/L_g$  evolution is under control, we can estimate the impact of individual deviations by replacing the sharp threshold on  $M_g$  with a soft threshold, substituting each galaxy mass  $M_g$  with  $M_g + \Delta M_g R$ , as in the previous section. This test was performed for samples as wide as those in our  $100 h^{-1}$  Mpc box and the effects of such replacement are modest, amounting to  $\sim 10\%$  of the difference found between  $\Lambda$ CDM and SUGRA.

Accordingly, the critical issue concerns the mean  $M_g/L_g$



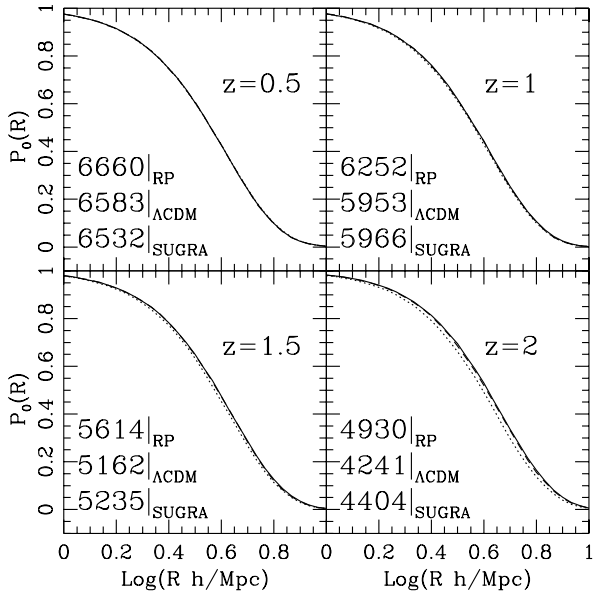


**Figure 7.** VPF's in comoving volumes for  $M_{tr} = 6 \cdot 10^{11} M_{\odot} h^{-1}$ . The four panels refer to redshift 0.5, 1, 1.5, 2, as indicated in the frames. The galaxy numbers in the simulation box are reported, for each model and redshift. Solid, dashed and dotted lines as in Fig. 6.

ratio. By comparing VPF's for different thresholds, we can however see that, in order that the shift of  $M_{tr}$  induces a VPF shift similar to differences between models,  $M_{tr}$  is to be displaced by a factor 1.7–1.8. Uncertainties  $\sim 10\%$  on the mean  $M_g/L_g$  ratio would therefore leave intact the discriminatory power of the VPF statistics.

Before concluding this section, let us finally comment on sample variance. All  $\Lambda$ CDM VPF's were estimated on the  $\Lambda$ CDM1 simulation. Differences between  $\Lambda$ CDM1 and  $\Lambda$ CDM2 are however small and could not be appreciated in the above plots. Accordingly, sample variance is not a relevant limit to the use of VPF's.

## 8 CONCLUSIONS

Dark Energy modifies the rate of cosmic expansion in the epoch when a substantial fraction of fluctuations on cluster scales reach their turnaround. Therefore, it seems quite natural to trace the redshift dependence of  $w(z) = p_{de}/\rho_{de}$  using the cluster mass function at different redshifts.

Unfortunately, the situation is more complicated. The evolution of  $w(z)$  affects observations in two ways. First, it causes objects to form and evolve with different rate. Second, it results in a different mapping of comoving coordinates of galaxies to observed angular positions and redshifts. Then, on a cluster mass scale ( $\sim 10^{14} h^{-1} M_{\odot}$ ), the evolutionary and geometrical effects tend to cancel, which makes clusters somewhat problematic for testing the equation of state.

In this paper we discuss the use of scales where the evolutionary effects are minimized, so that the geometrical effects leave a clearer imprint. In a sense, this is not a new procedure: an analogous idea is utilized when the DE equa-

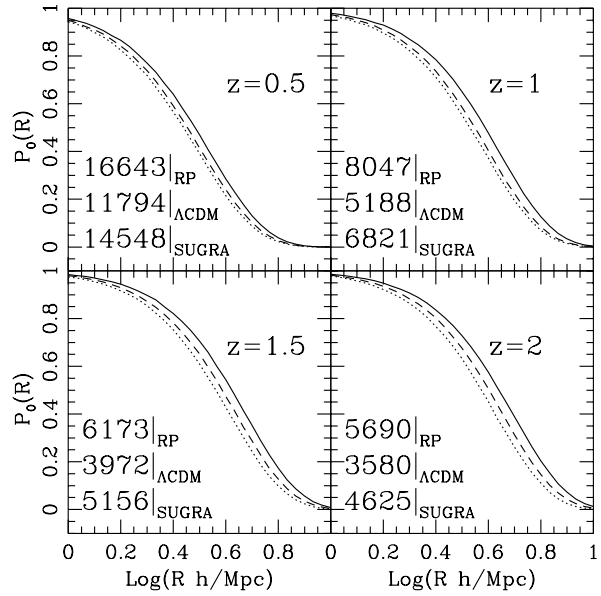


**Figure 8.** VPF's in comoving volumes for fixed angular density. The four panels refer to redshift 0.5, 1, 1.5, 2, as indicated in the frames. Numbers in the frames as in Fig. 7. Solid, dashed and dotted lines as in Fig. 6.

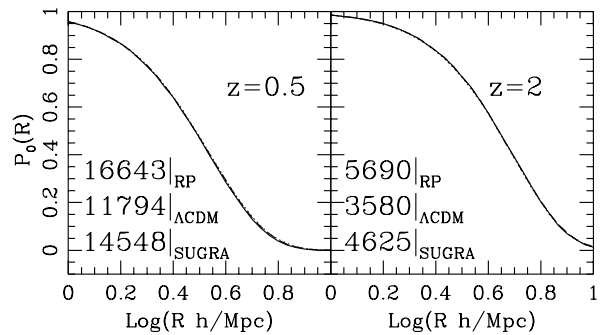


**Figure 9.** VPF's in fiducial volumes for fixed angular density. Numbers in the frames as for Fig. 7. Solid, dashed and dotted lines as in Fig. 6.

tion of state is tested by using a *standard candle*. Obviously, galaxies are not standard candles themselves, but they can provide a “standard meter” through their (almost) model-independent abundance and evolution.

Previous analysis, which focused on clusters, tried to overcome the above difficulties by making recourse to various features. For example, the evolutionary dependence on  $w$  is preserved if one considers masses *well* above  $10^{14} h^{-1} M_{\odot}$ . Unfortunately, clusters with masses  $\sim 10^{15} h^{-1} M_{\odot}$  or larger are rare today and surely are even more rare in the past. Some analysis (see, *e.g.*, Haiman et al. 2000) stressed a possible role of very massive clusters at large  $z$ . Yet, the number of such clusters cannot be large and, thus, comparing such predictions with observations is a hard challenge. There is also another problem with using cluster masses. Usually the mass function is estimated with a PS-like approximations,

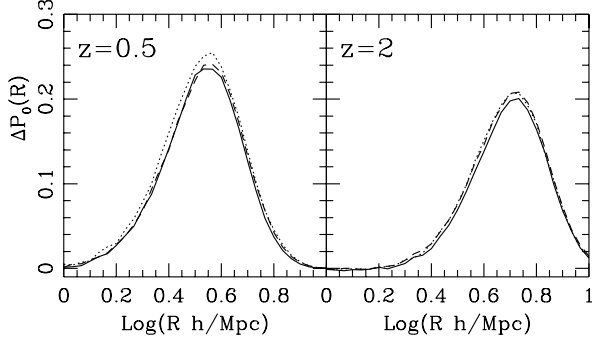


**Figure 10.** Differences between VPF’s of various models and the VPF for a Poisson sample, in fiducial volumes for fixed angular density. They arise from the sum of  $n$ -point correlation functions in eq. (26). Tiny residual differences between models, almost unappreciable in the previous plot, arise from differences between their  $n$ -point functions, clearly almost erased by geometrical renormalization.

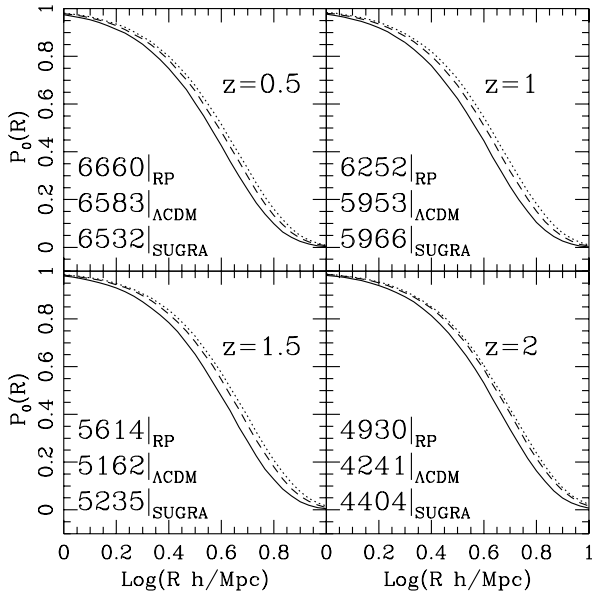


**Figure 11.** VPF’s in fiducial volumes for fixed mass limit (see text). Numbers in the frames as for Fig. 7. Solid, dashed and dotted lines as in Fig. 6.

which are well tested with simulations. The “virial” radius  $R_v$  is defined so that inside  $R_v$  the density contrast is  $\Delta_v$ . The value of  $\Delta_v$  depends on the redshift and on DE model. On the contrary, data are typically analyzed with a standard density contrast  $\Delta_c \simeq 180$  (or 200). Increasing  $\Delta_c$  reduces the amplitude of the mass function. If mass functions defined with variable  $\Delta_v$  (almost) overlap one another, mass functions defined with constant  $\Delta_c$  can be different. In order to account for these differences in the definitions, one needs to assume some shape for the density profile in the outskirts of clusters. This is typically done by using a NFW profile with concentration  $c_s \simeq 5$ . As we deal with rather peripheral (virial) cluster regions, we can neglect the spread of actual values of concentration. However, when different  $w(z)$  are

considered, the *mean*  $c_s$  changes substantially, up to 80% (Klypin et al 2003; Kuhlen et al. 2005). The differences between  $M_{200}$  and  $M_v$  are not large – 10–15%. Approximately the same percent of the difference depends on  $w$ . This may be still important. Neglecting these corrections may lead to substantial systematic errors.

As an alternative to using galaxy clusters, so avoiding these and other problems, here we suggest to exploit the dependence on DE nature of the redshift distribution of galaxies and argue that the difficulties of this approach can be overcome.

A first problem is that one needs to know how to treat subhalos of more massive halos because a large fraction of galaxies is hosted by subhalos. To populate massive halos with galaxies we use recent results on the halo occupation distribution (HOD). Accordingly, we believe that this difficulty can be readily overcome.

Dealing with galaxies also requires knowledge of their masses  $M_g$ . The  $M_g - L_g$  relation is more complex than the relation between  $M_v$ , X-ray flux and  $T$  in clusters.

Galactic evolution studies and/or techniques aiming to compare dynamical or lensing masses with luminosities can be used to this aim (Bressan et al 1994, Portinari et al 2004, Prada et al 2003). It is also known that there is no one-to-one correspondence between  $L_g$  and  $M_g$ , as the luminosities of two galaxies of the same mass can be quite different, up to one order of magnitude. We then considered separately two different issues: (i) How well we must know the evolution of  $\langle M_g/L_g \rangle_{L_g}$ . (ii) Which can be the impact of fluctuations about such average value, taking into account that the distribution about average can depend on  $z$  and mass.

How precisely  $\langle M_g/L_g \rangle_{L_g}$  is to be known, in order that different cosmologies can be safely discriminated, is shown by Fig. 6, according to Sec. 6: If we double the values of  $\delta\theta_{gg}/\theta_{gg}$  provided there, we have a fair estimate the evolution rate  $\mathcal{R} = \langle M_g/L_g \rangle_{L_g}(z)/\langle M_g/L_g \rangle_{L_g}(z=0)$  just covering the differences between models. Typically, if the estimated  $\langle M_g/L_g \rangle_{L_g}$  evolution is reliable at a  $\sim 10\%$  level, different models could be discriminated.

To reach this goal, fresh observational material is needed, but no conceptual difficulty is apparently involved in its acquisition.

The spread of the  $M_g/L_g$  ratio, around its average value, also involves a delicate issue, as it could cause systematics. Here we reported the effect of a random spread of  $L_g$  in a luminosity interval  $L_1, L_2$  with  $L_2 \simeq 20L_1$ . If the physical distribution of luminosities, for any mass and at any redshift, is within these limits, then possible systematics are well within errors due to other effects.

Further tests on  $L_g$  spread were also performed, which are not reported in detail in this paper. They apparently indicate that really wide and *ad-hoc* distributions are necessary, in order that possible systematics exceed Poisson uncertainty.

Although bearing these reserves in mind, we conclude that estimates of the redshift dependence of the average  $M_g/L_g$ , reliable within  $\sim 10\%$ , can enable us to obtain a fair information on DE nature.

In this paper we also discuss various tests based on the void probability function. We find that the VPF is almost model independent when estimated for samples with constant angular number density of galaxies. This result ap-

parently suggests that  $n$ -point functions are almost model independent, at any  $z$ , once distances are suitably rescaled. If the mean  $M_g/L_g$  evolution is under control, at the 10% level, we can also assess that VPF, for samples defined with a given  $M_{tr}$ , puts in evidence geometrical differences between models and provides a discriminatory statistics.

Combining the simulated halo distribution with the HOD provides an effective tool for testing the equation of state of DE. More work is needed to define the  $L_g$ - $M_g$  relation and, possibly, to reduce systematic effects. It is justified to expect that the  $z$ -dependence of galaxy distribution, in deep galaxy samples, will allow us to constrain the DE nature even more reliably than the density of galaxy clusters in future compilations, sampling them up to large  $z$ 's.

**Acknowledgments:** We thank Loris Colombo and Cesare Chiosi for stimulating discussions. An anonymous referee is also to be thanked for improving the arguments now in Sec. 6. A.K. acknowledges financial support of NSF and NASA grants to NMSU. S.G. acknowledges financial support by DAAD. Our simulations were done at the LRZ computer center in Munich, Germany.

## APPENDIX A: DYNAMICAL DARK ENERGY MODELS

Dynamical DE is to be ascribed to a scalar field,  $\phi$ , self-interacting through an effective potential  $V(\phi)$ , whose dynamics is set by the Lagrangian density:

$$\mathcal{L}_{DE} = -\frac{1}{2}\sqrt{-g}(\partial^\mu\phi\partial_\mu\phi + V(\phi)) . \quad (\text{A1})$$

Here  $g$  is the determinant of the metric tensor  $g_{\mu\nu} = a^2(\tau)dx_\mu dx_\nu$  ( $\tau$  is the conformal time). In this work we need to consider just a spatially homogeneous  $\phi$  ( $\partial_i\phi \ll \dot{\phi}$ ;  $i = 1, 2, 3$ ; dots denote differentiation with respect to  $\tau$ ); the equation of motion is then:

$$\ddot{\phi} + 2\frac{\dot{a}}{a}\dot{\phi} + a^2\frac{dV}{d\phi} = 0 . \quad (\text{A2})$$

Energy density and pressure, obtained from the energy-momentum tensor  $T_{\mu\nu}$ , are:

$$\rho = -T_0^0 = \frac{\dot{\phi}^2}{2a} + V(\phi) , \quad p = \frac{1}{3}T_i^i = \frac{\dot{\phi}^2}{2a} - V(\phi) , \quad (\text{A3})$$

so that the state parameter

$$w \equiv \frac{p}{\rho} = \frac{\dot{\phi}^2/2a - V(\phi)}{\dot{\phi}^2/2a + V(\phi)} \quad (\text{A4})$$

changes with time and is negative as soon as the potential term  $V(\phi)$  takes large enough values.

The evolution of dynamical DE depends on details of the effective potential  $V(\phi)$ . Here we use the model proposed by Ratra & Peebles (1988), that yield a rather slow evolution of  $w$ , and the model based on supergravity (Brax & Martin 1999, 2001; Brax, Martin & Riazuelo 2000). The latter gives a much faster evolving  $w$ . The RP and SUGRA potentials

$$V(\phi) = \frac{\Lambda^{4+\alpha}}{\phi^\alpha} \quad RP, \quad (\text{A5})$$

$$V(\phi) = \frac{\Lambda^{4+\alpha}}{\phi^\alpha} \exp(4\pi G\phi^2) \quad SUGRA \quad (\text{A6})$$

cover a large spectrum of evolving  $w$ . These potentials allow tracker solutions, yielding the same low- $z$  behavior that is almost independent of initial conditions. In eqs. (A5) and (A6),  $\Lambda$  is an energy scale in the range  $10^2$ - $10^{10}$  GeV, relevant for the physics of fundamental interactions. The potentials depend also on the exponent  $\alpha$ . Fixing  $\Lambda$  and  $\alpha$ , the DE density parameter  $\Omega_{de,o}$  is determined. Here we rather use  $\Lambda$  and  $\Omega_{de,o}$  as independent parameters. In particular, numerical results are given for  $\Lambda = 10^3$  GeV.

The RP model with such  $\Lambda$  value is in slight disagreement with low- $l$  multipoles of the CMB anisotropy spectrum data. Agreement may be recovered with smaller  $\Lambda$ 's, which however loose significance in particle physics. The SUGRA model considered here, on the contrary, is in fair agreement with all available data.

## REFERENCES

- Battye R. A. & Weller J., 2003, Phys.Rev., D68, 083506  
 Benson A. J., 2001, MNRAS, 325, 1039  
 Benson A. J., Baugh C. M., Cole S., Frenk C. S., Lacey C. G., 2000a, MNRAS, 316, 107  
 Benson A. J., Cole S., Frenk C. S., Baugh C. M., Lacey C. G., 2000b, MNRAS, 311, 793  
 Benson A. J., Frenk C. S., Baugh C. M., Cole S., Lacey C. G., 2003, MNRAS, 343, 679  
 Berlind A. A., Weinberg D. H., 2002, ApJ, 575, 587  
 Berlind A. A. et al., 2003, ApJ, 593, 1  
 Brax P. & Martin J., 1999, Phys.Lett., B468, 40  
 Brax P. & Martin J., 2000, Phys.Rev. D, 61, 103502  
 Brax P., Martin J. & Riazuelo A., 2000, Phys.Rev. D, 62, 103505  
 Bressan A., Chiosi C. & Fagotto F., 1994, ApJS, 94, 63.  
 Bryan G.L. & Norman M.L., 1998, ApJ 495, 80  
 Bullock J. S., Wechsler R. H., Somerville R. S., 2002, MNRAS, 329, 246  
 De Bernardis P. et al., 2000, Nature 404, 955  
 Dolag K., Bartelmann M., Perrotta F., Baccigalupi C., Moscardini L., Meneghetti M., Tormen G., 2004, A&A, 416, 853  
 Dvali G., & Turner M., 2003, astro-ph/0301510  
 Efstathiou G. et al., 2002, MNRAS, 330, 29  
 Governato F., Baugh C. M., Frenk C. S., Cole S., Lacey C. G., Quinn T., Stadel J., 1998, Nature, 392, 359  
 Haiman Z., Mohr J. J. & Holder G. P., 2000, ApJ, 553, 545  
 Halverson N. W. et al., 2001 ApJ, 568, 38  
 Hanany S. et al., 2000, ApJ, 545, L5  
 Huterer D. & White M., 2002 ApJ, 578, L95  
 Jenkins A. et al., 2001, MNRAS, 321, 372  
 Kauffmann G., Nusser A., Steinmetz M., 1997, MNRAS, 286, 795  
 Kauffmann G., Colberg J. M., Diaferio A., White S. D. M., 1999a, MNRAS, 303, 188  
 Kauffmann G., Colberg J. M., Diaferio A., White S. D. M., 1999b, MNRAS, 307, 529  
 Klypin A., Macciò A.V., Mainini R., Bonometto S.A. 2003 ApJ, 599, 31  
 Knebe A., Kravtsov A. V., Gottloeber S., Klypin A., 2000, MNRAS, 317, 630  
 Kravtsov A., Klypin A. & Khokhlov A., 1997 ApJ, 111, 73  
 Kravtsov A. V., Berlind A. A., Wechsler R. H., Klypin A. A., Gottloeber A., Allgood B., Primack J. R., 2004, ApJ, 609, 35  
 Kuhlen, M., Strigari, L. E., Zentner, A. R., Bullock, J. S., & Primack, J. R. 2005, MNRAS, 357, 387  
 Linder E.V. & Jenkins A. 2003, MNRAS, 346, 573  
 Macciò A. V., 2005, MNRAS, 361, 1250  
 Macciò A. V., Governato F., Horellou C., 2005, MNRAS, 359, 941  
 Magliocchetti M., Porciani C., 2003, MNRAS, 346, 186

- Mainini R., Macciò A. V., Bonometto S. A., 2003a, *NewAst.*, 8, 173
- Mainini R., Macciò A. V., Bonometto S. A., Klypin A., 2003b *ApJ*, 599, 24
- Majumdar S. & Mohr J. J., 2004, *ApJ*, 613, 41
- Nagamine K., Fukugita M., Cen R., Ostriker J. P., 2001, *ApJ*, 558, 497
- Pearce F. R., Jenkins A., Frenk C. S., White S. D. M., Thomas P. A., Couchman H. M. P., Peacock J. A., Efstathiou G., 2001, *MNRAS*, 326, 649
- Percival W. J. et al., 2002, *MNRAS*, 337, 1068
- Perlmutter S. et al., 1999, *ApJ*, 517, 565
- Portinari L., Sommer-Larsen J. & Tantalò R., 2004, *MNRAS*, 347, 691
- Prada F., Vitvitska M., Klypin A., Holtzman J.A., Schlegel D.J., Grebel E.K., Rix H.-W., Brinkmann J., McKay T.A., Csabai I., 2003, *ApJ*, 598, 260
- Press W. H. & Schechter P., 1974, *ApJ*, 187, 425
- Ratra B., Peebles P. J. E., 1988, *Phys.Rev.D*, 37, 3406
- Riess, A. G. et al., 1998, *AJ*, 116, 1009
- Seljak U., 2000, *MNRAS*, 318, 203
- Sheth R. K. & Tormen G., 1999, *MNRAS*, 308, 119
- Sheth R. K. & Tormen G., 2002, *MNRAS*, 329, 61
- Sheth R. K., Diaferio A., 2001, *MNRAS*, 322, 901
- Somerville R. S., Lemson G., Sigad Y., Dekel A., Kauffmann G., White S. D. M., 2001, *MNRAS*, 320, 289
- Spergel D. N. et al., 2003, *ApJsuppl.*, 148, 175
- Tegmark, M., Zaldarriaga, M., Hamilton, A. J., 2001, *Phys. Rev.D*, 63, 43007
- Vale A. & Ostriker J.P., 2004, *MNRAS*, 353, 189V
- van den Bosch F.C, Yang X.H. & Mo H.J., 2003, *MNRAS*, 340, 771
- Wang L. & Steinhardt P.J., 1998, *ApJ*, 508, 483
- Wechsler R. H., Somerville R. S., Bullock J. S., Kolatt T. S., Primack J. R., Blumenthal G. R., Dekel A., 2001, *ApJ*, 554, 85
- Wetterich C., 1988, *Nucl.Phys.B*, 302, 668
- Wetterich C., 1995 *A&A* 301, 32
- White M., Hernquist L., Springel V., 2001, *ApJ*, 550, L129
- Yang X.H., Mo H.J. & van den Bosch F.C, 2003, *MNRAS*, 339, 1057
- Yang X.H., Mo H.J., Jing Y.P., van den Bosch F.C & Chu Y., 2004, *MNRAS*, 350, 1153
- Yoshikawa K., Taruya A., Jing Y. P., Suto Y., 2001, *ApJ*, 558, 520
- Zheng Z., Tinker J. L., Weinberg D. H., Berlind A. A., 2002, *ApJ*, 575, 617